JOURNAL OF MAGNETIC RESONANCE, Series A 116, 59–66 (1995)

Orientation-Selected 95 GHz High-Field ENDOR Spectroscopy of Randomly Oriented Plastoquinone Anion Radicals

M. ROHRER,* M. PLATO,* F. MACMILLAN,† Y. GRISHIN,‡ W. LUBITZ,† AND K. MÖBIUS*,§

*Institut für Experimentalphysik, Freie Universität Berlin, Arnimallee 14, D-14195 Berlin, Germany; †Max-Volmer-Institut für biophysikalische und physikalische Chemie, Technische Universität Berlin, Strasse des 17. Juni 135, D-10623 Berlin, Germany; and ‡Institute of Chemical Kinetics, Russian Academy of Sciences, 630090 Novosibirsk, Russia

Received January 13, 1995; revised March 10, 1995

Recent improvements of a 3 mm high-field/high-frequency CW EPR/ENDOR spectrometer [O. Burghaus, M. Rohrer, T. Götzinger, M. Plato, and K. Möbius, *Meas. Sci. Technol.* 3, 765 (1992)] are presented, making it possible for ENDOR measurements to be performed with NMR radiofrequency fields of more than 2.5 mT (rotating frame) over a frequency range of 40 MHz. Applications of this setup to plastosemiquinone anion radicals are described which serve as a model for the secondary electron acceptor in plant photosystem II. The orientation-selected high-field ENDOR spectra of the plastoquinone anion radicals, recorded at different EPR field positions, are analyzed with the aid of computer simulations. The determination of hyperfine interactions of the radical in a perdeuterated solvent is described. The experiments demonstrate the potential of high-field/high-frequency EPR/ENDOR in structure determination including anisotropic interactions with the environment.

INTRODUCTION

Electron–nuclear double resonance spectroscopy of randomly oriented paramagnetic systems allows hyperfine measurements for selected molecular orientations that correspond to the principal axes of the g tensor. This Zeeman magnetoselection was first applied by Rist and Hyde in 1970 (*1*) and since then has been used to great advantage in ENDOR studies of transition metal complexes, i.e., metalloproteins and enzymes [for recent reviews, see (*2, 3*)]. In these systems, the g-tensor anisotropy is large enough to achieve considerable orientation selectivity already for the Zeeman fields of X-band EPR/ENDOR (9.5 GHz). For many bioorganic radicals, however, the g-tensor anisotropy is much smaller and, consequently, the Zeeman magnetoselection at X-band EPR is often insufficient to select distinct orientations. A solution to this problem is offered by high-field/high-frequency EPR and ENDOR spectroscopy operating, for example, at 10 times higher microwave frequencies and Zeeman fields (W band, 95 GHz). This allows single-crystal-like ENDOR spectra to be taken from disordered samples even with very small g-tensor anisotropies [for recent reviews on high-field EPR and ENDOR, see (*4, 5*)].

In recent years, we have applied high-field EPR and ENDOR to photosynthetic donor and acceptor pigments and their biomimetic model systems. For this purpose, a 95 GHz CW EPR/ENDOR spectrometer was built (*6–8*). Most recently, it has been extended to pulsed EPR and ENDOR capability with a heterodyne detection scheme (*9*). In this paper, considerable improvements of the radiofrequency part of the ENDOR setup are described, which allow B_2 fields of more than 2.5 mT (rotating frame) to be generated over a frequency range of 40 MHz around 145 MHz with a minimum of unwanted RF power reflections and stray fields.

The new RF configuration is currently used to perform ENDOR experiments on semiquinone anion radicals as models for acceptor molecules in photosynthesis. Here, we restrict ourselves to the plastoquinone-1 (PQ-1: 2,3-dimethyl-5-(3-methylbut-2-enyl)-1,4-benzoquinone) which serves as a model for the plastoquinone acceptor in plant photosystem II (*10*):

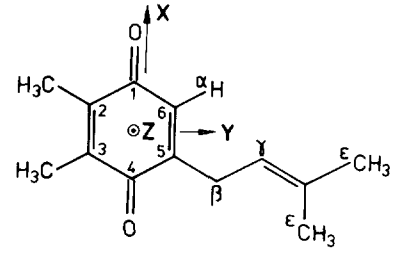

EXPERIMENTAL

General CW ENDOR Scheme

In Fig. 1, the simplified block diagram of the present CW EPR/ENDOR setup is shown. The cavity is of the cylindrical TE_{011} type. Details are given in the figure caption; see also Ref. (*6*). Additional X-band EPR/ENDOR measurements were performed on a Bruker ER 200-D spectrometer with the standard Bruker cavity ENB 200.

§ To whom correspondence should be addressed.

1064-1858/95 $12.00

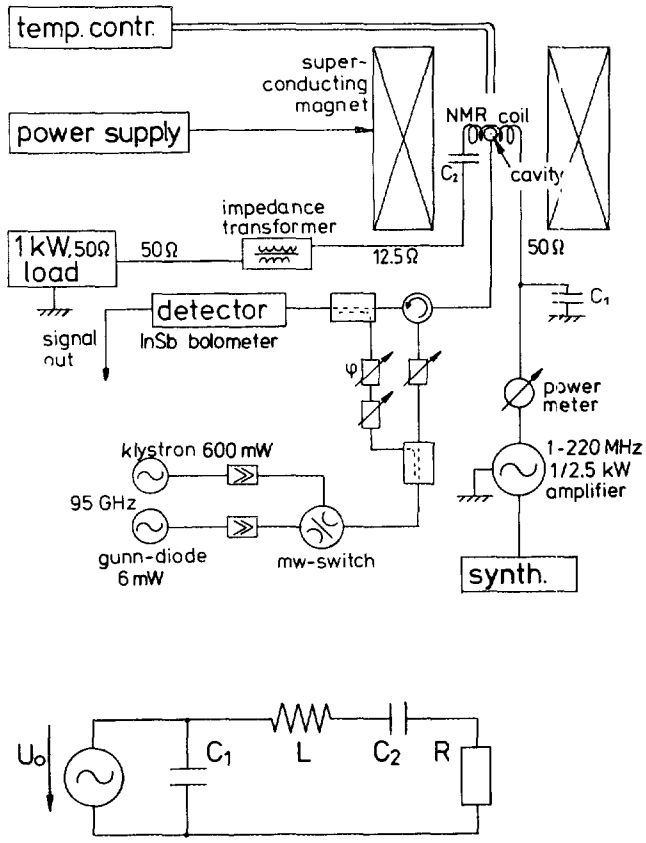

FIG. 1. (Top) Simplified block diagram of the present W-band EPR/ENDOR setup (CW version) at the FU Berlin including the new improved version of an RF circuit: NMR coil with four loops, surrounding the ENDOR TE_{011} cavity (*27*). Two capacitors C_1 and C_2 in parallel and in series, respectively; 1 kW 50 Ω load resistor connected with a 4:1 impedance transformer and a 12.5 Ω transmission line to the RF circuit. Further details were described previously (*6*). (Bottom) Simplified RF scheme with two capacitors, NMR coil, and resistor. See also legend to Fig. 2.

Radiofrequency Circuit

Experimental problems concerning the generation of strong NMR RF fields (B_2) under the specific conditions of an ENDOR experiment have been described in the literature (*11, 12*). The high-static Zeeman field B_0 of about 3.4 T, at which a 95 GHz (W band) ENDOR experiment is performed, shifts the nuclear Larmor frequencies to values 10 times higher than those at X-band ENDOR, e.g., for protons from 14.4 to 144 MHz. This considerably increases the RF stray field problems. Furthermore, when increasing B_0, the geometrical requirements of an NMR coil are also changed (*6*). Consequently, technical solutions obtained for X-band ENDOR generally cannot directly be transferred to W-band ENDOR configurations.

The simplest way to connect an ENDOR coil to an RF amplifier is by short-circuiting it to the source. This combines the advantages of a very simple RF scheme and of producing high B_2 fields by a high current through the NMR coil. On the other hand, an NMR coil in short circuit leads to strong reflections of the power back into the RF amplifier output.

The problem of optimizing the matching between NMR coil and RF amplifier can be treated by means of the complex impedance $Z = R + i(\omega L - 1/\omega C)$, in which R is the real resistance, $(\omega L - 1/\omega C)$ the reactance, L the inductance, C the capacity, and ω the angular RF frequency. The reflection coefficient can be written as $r = (Z_L - Z_T)/(Z_L + Z_T)$, where Z_L and Z_T are the impedances of the load (L) and the transmission line (T) between the load and the amplifier output, respectively. For a load with a pure reactance, represented by a coil with neglegible R, no impedance matching to the output of an RF source is possible at all.

In order to avoid standing waves by reflection, which may result in destructive interferences in the transmission line, the coaxial cable has to be shorter than $\lambda/4$. Even in this case, a short circuit still has the disadvantage that the reflected power can lead to damage and/or decreased lifetime of the power stages of the amplifier and to disturbing stray RF fields in the laboratory. In addition, the mismatched circuit suffers from strong nonlinearity between frequency and B_2 amplitude.

Impedance matching of the NMR coil to the RF amplifier output over the required frequency band can be realized by introducing a real resistance into the RF circuit. Several impedance-matching networks for more or less broad frequency bands have been described using *RL* and *RLC* circuits (*11–15*). Capacitive elements are introduced to compensate for the inductive reactance of the NMR coil. The use of resonant *LC* schemes provides an enhanced B_2 field at the resonant frequency $\omega_r = (LC)^{-1/2}$. A sophisticated arrangement using a parallel *LC* circuit is described by Pfenninger (*13*). A chain of impedance transformers matches a tunable *LC* circuit with an impedance of about 3200 Ω. This network allows the current in the coil to be enhanced by q values of 20 and more (where q is defined as the resonant frequency divided by the full width at half maximum of the resonant curve). Synchronous tuning of the circuit while sweeping the ENDOR frequency is necessary and is achieved by phase monitoring and mechanically changing the capacity according to the resonance condition.

The network chosen for our present W-band ENDOR experiments is a less complicated compromise between impedance matching and resonant RF current enhancement. It contains a *series RLC* circuit driven into resonance at *low* impedance. According to $q = (L/C)^{1/2}/R$, where the inductance L of the NMR coil can only be varied in narrow limits, the q value is approximately 1 or 2, depending on the choice between a coil with two or four loops (47 or 115 nH, respectively), when a resistance of 50 Ω (equivalent to the output impedance of the RF amplifier) and a center frequency of about 145 MHz are kept fixed. Considering the organic molecules we want to study (with hyperfine couplings less than 20 MHz), we strive for high B_2 fields even at the

expense of narrowing the bandwidth of the impedance matching and of the linearity range. Consequently, the q value of the circuit is increased by reducing R. This is realized by an impedance transformer (4:1), which is connected to the LC circuit with a 12.5 Ω transmission line and to an RF power resistor (Bird Model 8251, 1 kW, 50 Ω) with a commercial 50 Ω cable (Suhner, RG-213 U 3025). In order to further optimize the characteristics of the circuit, a second capacitor in parallel is introduced. It leads to a second resonance and to characteristics of the circuit comparable to those of a π filter. The complete matching network is shown in Fig. 1 (bottom).

The resulting q value of about 4 (using an NMR coil with four loops) can be extracted from the frequency response function in Fig. 2, where the frequency-dependent B_2 fields as well as the reflection function, both measured and calculated for the network (optimized for proton ENDOR), are shown. In the calculations, losses of about 5 Ω are included, which are mainly caused by the increased resistances of the elements by the skin effect at high RF frequencies.

Sample Preparation

The synthesis of plastoquinone-1 (2,3,-dimethyl-5-(3-methylbut-2-enyl)-1,4-benzoquinone) was performed according to procedures adapted from the literature (*16*). A large excess of 2,3-dimethylhydroquinone (which served as the starting material) reacted with 2-methyl-3-buten-2-ol in the presence of boron trifluoride-etherate in 1,4-dioxan. The alkylated hydroquinone was formed quickly and then oxidized to the quinone by using silver oxide. The product was purified by silica gel column chromatography. Final purification of PQ-1 was done by vacuum sublimation. The purity and structure of PQ-1 were confirmed by MS and NMR spectroscopy (*24*).

The PQ-1 anion radical was generated by dissolving the quinone ($\approx 10^{-3} M$) in slightly basic (K-t-BuO) solution of fully deuterated isopropanol. The solution was degassed by bubbling with purified argon for a few minutes and then frozen in liquid nitrogen.

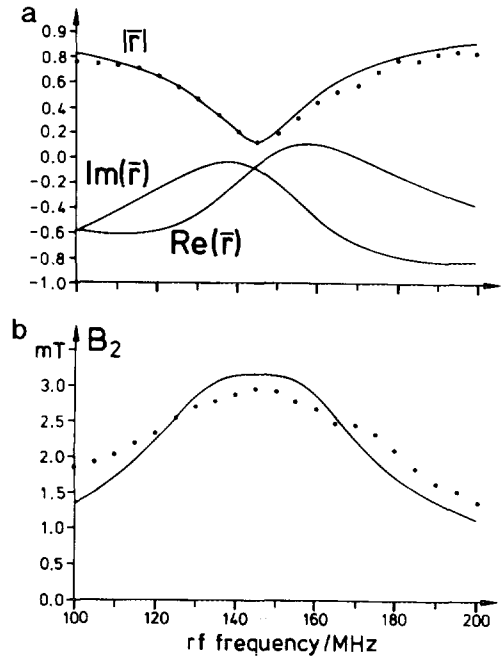

FIG. 2. Properties of the RF-circuit: The complex impedance is given by

$$Z(\omega) = (1/i\omega C_1)[(1/i\omega C_2) + i\omega L + R)/(R + i\omega L + (1/i\omega)(1/C_1 + 1/C_2)]$$

from which the real and imaginary parts of the impedance can be deduced to calculate the reflection and current in the circuit. (a) The complex frequency-dependent reflection function r (modulus, real, and imaginary parts) of the RF circuit calculated with C_1 = 35 pF, C_2 = 16 pF, L = 95 nH, and R = 17.5 Ω. Additional losses of the elements decrease the quality factor of the circuit. The dots represent measured values determined with a matched directional coupler and a 400 MHz oscilloscope. (b) Frequency dependence of B_2 field strength (rotating frame) calculated for a constant input power of 2.5 kW, a rectangular coil with four loops (0.28 mT/A) and other values as above. The measured points were determined by a calibrated pickup coil (2 mm diameter), a constant input power of 32 mW and scaled to the maximum output power (2.5 kW) of the RF amplifier in the pulsed mode (duty cycle ≤ 15%). The RF attenuation of the slotted TE_{011} cavity is less than 1 dB and not included in the calculation.

SIMULATION OF ENDOR SPECTRA OF RANDOMLY ORIENTED RADICALS

The EPR spectra of randomly oriented molecules, such as radicals in frozen solution or powder samples, result from superpositions of signals from all molecular orientations with respect to the direction of the static magnetic field (*17*). For doublet-state organic radicals, the spin Hamiltonian can be written as

$$\mathcal{H} = \beta B_0 \hat{\mathbf{g}}\mathbf{S} + h \sum_{i=1}^{n} \mathbf{S}\hat{\mathbf{A}}^{(i)}\mathbf{I}_i - g_n\beta_n B_0 \sum_{i=1}^{n} \mathbf{I}_i, \qquad [1]$$

where β is the Bohr magneton, $\hat{\mathbf{g}}$ the g tensor, h the Planck constant, B_0 the external field, and $\hat{\mathbf{A}}^{(i)}$ are the hyperfine tensors. S and I are the electron- and nuclear-spin vector operators, and g_n and β_n are the nuclear g factor and magneton, respectively. Since, in this study, we are observing only hyperfine interactions with protons ($I = \frac{1}{2}$), quadrupolar terms are omitted in Eq. [1].

Depending on the anisotropy of the g tensor and the magnitude of B_0, a more or less well-determined selection of specific orientations of the radicals is provided by the electron Zeeman term: Each field value of an EPR spectrum dominated by g anisotropy represents one set of molecular orientations with respect to the magnetic-field direction (*17*). Thus, by performing ENDOR at several field positions, the angular dependence of the hyperfine interaction can be measured. For a sufficiently large anisotropy of the Zeeman in-

teraction (i.e., if $\Delta g B_0 >$ inhomogeneous linewidth ΔB), even single-crystal-like ENDOR spectra can be recorded at the turning points of the EPR powder pattern and, under favorable symmetry conditions, hyperfine tensors can be determined in the g-axes system (*18, 19*).

The field B_0 in X-band experiments is around 0.3 T and allows orientational selection only when the g anisotropy is at least 10^{-2} assuming linewidths $\Delta B < 3$ mT. Such favorable situations are typical for transition-metal complexes, for which orientation-selective ENDOR was performed to determine ligand positions from hyperfine interactions (*3*).

Taking advantage of the 10-times-higher Zeeman interaction at 95 GHz EPR, one can perform angle-selective ENDOR measurements of randomly oriented radicals even with g anisotropies as small as 10^{-3}, which remain unresolved in most X-band EPR experiments.

It should be pointed out that all field positions of an EPR powder spectrum represent manifolds of molecular orientations, except for the turning points (two for orthorhombic g tensors, one for axial g tensors). Consequently, the ENDOR spectra also show superpositions of selected sets of orientations. Especially when recording ENDOR spectra of more than one hyperfine coupling, one often obtains strongly overlapping lines. Moreover, if the hyperfine anisotropies are very small, it becomes increasingly difficult to distinguish the ENDOR lines from different orientations. Additional problems arise when the hyperfine-tensor axes are not collinear with the g-tensor axes. On the other hand, the relative orientation of hyperfine interactions in the g-tensor axes system is often of particular interest, since it contains useful information about anisotropic interactions with the environment, such as hydrogen bonding (*20*).

In order to extract a maximum of information from angle-selective ENDOR spectra, advanced methods of computer simulation have been developed and successfully applied (*18*). Since the electron Zeeman interaction is the dominating term in the spin Hamiltonian, the principal-axis system of the g tensor is chosen as the molecular reference frame. Expressing the magnetic field direction in this system by spherical coordinates θ, ϕ, the direction cosines are

$$h_1 = \cos\phi \sin\theta,\ h_2 = \sin\phi \sin\theta,\ h_3 = \cos\theta. \quad [2]$$

Introducing the principal values g_k, the angle-dependent g-factor function $g(\theta, \phi)$ is given by (*17*)

$$g(\theta, \phi) = [\sum_{k=1}^{3} (g_k h_k)^2]^{1/2} \quad [3]$$

and the hyperfine splitting of one particular set of nuclei is

$$A(\theta, \phi) = \sum_{j=1}^{3} (\sum_{k=1}^{3} g_k h_k A_{kj} h_j)/g(\theta, \phi), \quad [4]$$

where A_{kj} are the elements of the hyperfine tensor in the g-axis system. This linearized form of $A(\theta, \phi)$ holds for the limiting case that the nuclear Larmor frequency $\nu_n = g_n \beta_n B_0/h \gg |A_{kj}|$, which is well fulfilled in W-band EPR/ENDOR of our organic radicals ($\nu_n \approx 140$ MHz, $|A_{kj}| \lesssim 10$ MHz) (*21*).

The orientation-dependent field positions $B_{res}(\theta, \phi)$ of the EPR signal for different sets i of nuclei are

$$B_{res}(\theta, \phi) = [\nu - \sum_{i=1}^{n} A^{(i)}(\theta, \phi) m_i] h/g(\theta, \phi)\beta, \quad [5]$$

where ν is the excitation microwave frequency and m_i are the magnetic spin quantum numbers of the nuclei. For the general case, where the g and hyperfine tensors are neither collinear nor axially symmetric, the tensor components in Eqs. [4] and [5] cannot be derived analytically. Consequently, numerical methods must be applied to calculate iteratively the relationship between resonant field positions and corresponding molecular orientations. In addition, for the general case of more than one dominant hyperfine coupling, all possible nuclear configurations must be taken into account with their resulting statistical weights.

For the final goal of simulating ENDOR spectra at any given position of an EPR powder spectrum, it is, unfortunately, not sufficient to collect only the sets of orientations at each field position as determined by the g anisotropy alone. As is obvious from Eq. [5], molecular orientations are, in general, selected not only by the g anisotropy, but also by the angle dependence of the hyperfine couplings. Neglecting this complication is an acceptable approximation only in cases where the anisotropic contributions to the electron Zeeman term are very large compared to all hyperfine interactions of the spin system. This specific condition is not fullfilled in the cases studied here, even at high-field 95 GHz EPR/ENDOR, and therefore the general case must be considered.

The ENDOR transition frequencies for doublet radicals in single-crystal or powder-type samples are most generally given by (*19*).

$$\nu_{ENDOR}^{(i)} = \{\sum_{j=1}^{3} [(m_s/g(\theta, \phi)) \times (\sum_{k=1}^{3} g_k h_k A_{kj}^{(i)}) - h_j \nu_n]^2\}^{1/2}, \quad [6]$$

where m_s is the magnetic electron-spin quantum number.

Equation [6] can easily be extended by additional quadrupolar terms. It was successfully applied in the treatment of ligand ENDOR of transition-metal complexes in randomly oriented samples (*18, 19*).

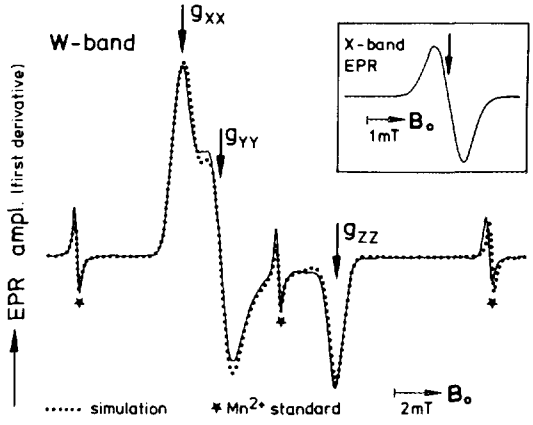

FIG. 3. EPR spectra (X/W band) of PQ-1$^{\cdot-}$. (Left) *Solid line:* W-band CW EPR spectrum of frozen solution of PQ-1$^{\cdot-}$ in perdeuterated isopropanol. Experimental conditions: temperature, 130 K; field modulation, ± 0.1 mT, 40 kHz; time constant, 1 s; 1 scan; acquisition time, 20 min. The three lines marked with * correspond to Mn^{2+} standard lines (*6, 20*). *Dotted line:* simulation by the program described in the text. Field positions, where ENDOR experiments were performed, are marked by arrows; they correspond to the principal values g_{XX}, g_{YY}, g_{ZZ}, respectively. (Inset) X-band CW EPR spectrum. Temperature and other conditions comparable with W-band experiment. The central field position (arrow) is fixed for the ENDOR experiment.

For $\nu_n \gg |A_{kj}|$ and small g anisotropies ($<10^{-2}$), Eq. [6] can be linearized to

$$\nu_{\mathrm{ENDOR}}^{(i)} = |\nu_n - m_s A^{(i)}(\theta, \phi)| \qquad [7]$$

with $A^{(i)}(\theta, \phi)$ as expressed by Eq. [4].

In the present work, the W-band ENDOR spectra are simulated using Eq. [7], whereas the X-band ENDOR simulations are based on the more general Eq. [6]. The ENDOR intensities for any chosen field position were convolved with the homogeneous EPR lineshape function.

ENDOR lineshapes were chosen to be Lorentzian. The ENDOR spectra were simulated with different linewidths and relative amplitudes for different hyperfine couplings, of which up to six can be included in our program. This accounts for different relaxation times for different hyperfine couplings, leading to a specific linewidth of a particular ENDOR line pair. Convolution of the ENDOR lineshapes is realized by algorithms of fast Fourier transformation (*22*). The typical CPU time on a DEC-Alpha 3300 workstation for one ENDOR simulation, built up from five hyperfine tensors, is about 1 min for an angular resolution of 1°.

The angular resolution (integration step width) of the calculations was set to 1° in both the polar and the azimuthal angles. The hyperfine principal axes X', Y', Z' and the g-tensor principal axes X, Y, Z were taken as collinear in the Z direction, but with a free angle Φ_0 in the X–Y plane, which is a symmetry plane of the π system of the molecule (*20*).

RESULTS AND DISCUSSION

In Fig. 3, the 9.5 GHz (X band) and 95 GHz (W band) EPR spectra of the plastosemiquinone anion radicals in frozen perdeuterated isopropanol are depicted. In addition, the EPR simulation of the W-band spectrum is shown. The higher Zeeman interaction at 95 GHz leads to a resolution of the g-tensor components g_{XX}, g_{YY} and g_{ZZ}. The g_{YY} component shows partially resolved hyperfine structure. The procedure of determining the g-tensor principal values by simultaneously recording an Mn^{2+} standard signal and computer simulating the EPR spectrum was described earlier (*20*). For the PQ-1 anion radical, we obtain $g_{XX} = 2.00610$, $g_{YY} = 2.00512$, and $g_{ZZ} = 2.00226$ (RMS error $\pm 3 \times 10^{-5}$). The assignment of the g-tensor components to the molecular reference system is the same as rationalized in Ref. (*20*).

The X-band ENDOR spectrum, recorded at the center of the corresponding EPR signal (Fig. 3 inset) is shown in Fig.

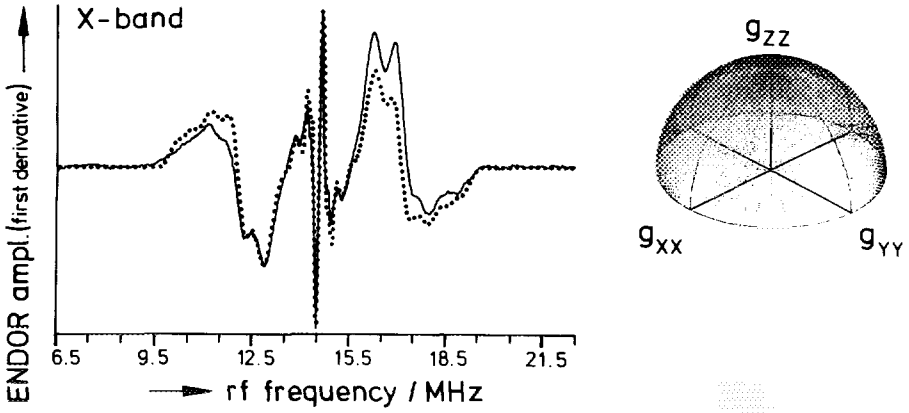

FIG. 4. X-band ENDOR spectrum of PQ-1$^{\cdot-}$. (Left) *Solid line:* CW ENDOR spectrum at 9.5 GHz, taken at the central field position as marked in Fig. 3 (inset). Experimental conditions: temperature, 125 K; RF modulation, 25 kHz; acquisition time, 80 min; RF power, 80 W. *Dotted line:* simulated ENDOR spectrum. For parameters, see text and Table 1. (Right) Schematic representation of the calculated angle selection as determined at the central EPR field position.

4, again together with its simulation and angle selection. Since the X-band EPR spectrum is not dominated by the g-tensor anisotropy, but rather by the hyperfine anisotropy (see text and Eqs. [1] and [5]), no angle selection is attempted in the wings of the spectrum, which might lead to misinterpretations (*25*). Obviously, all molecular orientations are involved and, accordingly, all hyperfine principal values contribute to the spectrum. Although the "single-crystal linewidth" at X band is narrower than at W band, reliable assignments of the hyperfine couplings can only be achieved by help of the W-band spectra.

In order to determine the hyperfine tensors with respect to the g-tensor principal-axis system, W-band ENDOR spectra were recorded at the g_{XX}, g_{YY}, and g_{ZZ} field positions; see Fig. 5. The ENDOR simulations and representations of the corresponding angle selections, as calculated by the program described, are also depicted. The spectra are calculated by

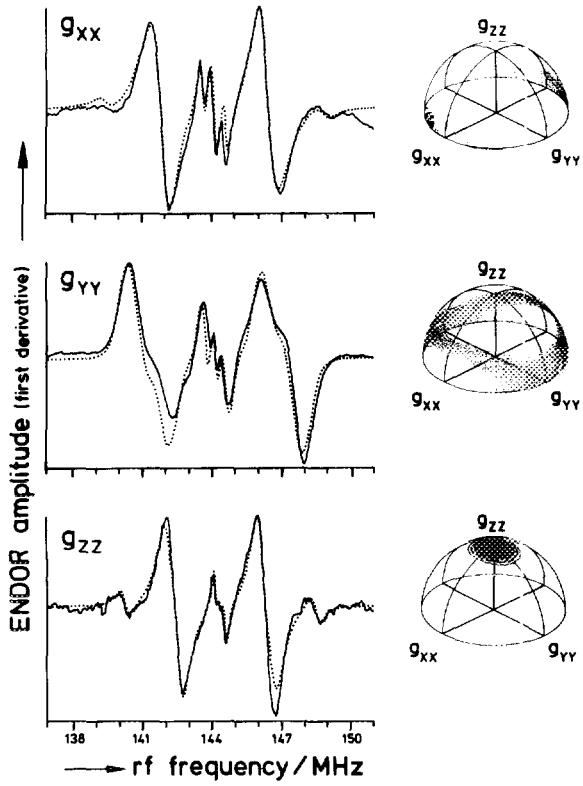

FIG. 5. W-band ENDOR spectra of PQ-1$^{\cdot-}$ at three g-tensor values for angle selections. (Left) *Solid lines:* W-band CW ENDOR spectra of frozen solution of PQ-1$^{\cdot-}$ in perdeuterated isopropanol taken at the three field positions marked in Fig. 3. They correspond to the directions of the principal axes of the g tensor with respect to the external field direction. Experimental conditions: temperature, 130 K; RF modulation, FM deviation, ±40 kHz, FM frequency, 18.5 kHz; time constant, 1 s; step width, 10 kHz; number of acquisitions, 4; acquisition time, 560 s (each spectrum); RF power, 220 W. *Dotted lines:* simulated ENDOR spectra. For parameters, see text and Table 1. (Right) Schematic representation of the calculated angle selections as determined at the EPR field positions of g_{XX}, g_{YY}, g_{ZZ}, respectively.

TABLE 1

Experimental g-Tensor and Principal Hyperfine-Tensor Components (in Megahertz) for Plastosemiquinone-1 Radical Anions in Frozen Perdeuterated Isopropanol

	$^2CH_3$	$^3CH_3$	^6H	$^4CH_3$	$^4CH_3$
$A_{X'X'}$	4.7(2)	3.9 (2)	9.3(3)	1.0(4)	0.8 (2)
$A_{Y'Y'}$	7.9(2)	6.8 (2)	0.2(—)*	1.0(—)*	0.5 (1)
$A_{Z'Z'}$	4.5(1)	3.50(8)	8.4(2)	1.6(5)	0.40(4)
Φ_0 (°)	17 (8)	12 (8)	12 (8)	*	*

g_{XX} = 2.00610(3), g_{YY} = 2.00512(3), g_{ZZ} = 2.00226(3).

Note. * indicates undetermined errors and Φ_0 values because of overcrowding lines. The principal axis Z' is assumed to be parallel to the principal g-tensor axis Z for symmetry reasons, Φ_0 is the angle between the principal axes X and X' (or Y and Y') in the XY symmetry plane. Values in brackets are 30% probability errors (see text). $^2CH_3$, $^3CH_3$, and $^4CH_3$ are methyl groups at position 2, 3, and 4, respectively. Principal axes for the latter methyl groups are not clearly defined because the isoprenoid chain can be locked in different conformations. For assignments of hyperfine tensors to molecular positions, see text.

one set of parameters that also fits the X-band ENDOR spectrum of PQ-1$^{\cdot-}$.

Table 1 gives the set of hyperfine principal values of the PQ-1$^{\cdot-}$ anion radical in perdeuterated isopropanol resulting from the W- and X-band ENDOR simulations. The X-band simulation was used to test consistency with the W-band results.

The errors (30% confidence range) in the last digit (in brackets) were obtained according to standard procedures (*23*) by inversion of the normal matrix, which is set up from the partial derivatives of the calculated spectrum with respect to the various parameters. Only the errors found along appropriate directions (e.g., X' for $A_{X'X'}$) are presented. The errors vary quite considerably depending on the sensitivity of the spectrum toward changes in the corresponding parameters. The error in the angle Φ_0 (between g_{XX} and $A_{X'X'}$, see above) turns out to be relatively large because it includes the uncertainty of the field positions (about 0.1 mT) where ENDOR was performed. Particularly along the Y direction, changes of the ENDOR field position by about 0.2 mT result in changes of the simulated spectra comparable to those occuring when the angle Φ_0 is changed by about 5°. This demonstrates the importance of a rigorous, although very time-consuming, error analysis when using quinones as spin probes for solute–solvent interactions in polycrystalline samples (e.g., in proteins). Obviously, the significance of environmental effects on the electronic structure of quinones can only be judged on the basis of reliable confidence ranges of the measured interaction parameters.

Assignments of hyperfine tensors to specific positions in the plastosemiquinone molecule (see the structural formula above) are based on expected magnitudes of corresponding

tensor components and on the observed temperature dependence of the ENDOR signal amplitudes (*1, 24*). The average values $\frac{1}{3}\mathrm{Tr}(\hat{\mathbf{A}})$ of the principal tensor components of the methyl groups at ring positions 1 and 2 and of the proton at position 6 are expected to be on the order of 6 MHz by referring to the isotropic proton hyperfine coupling constant of benzoquinone$^{\cdot -}$ (*20*). This leads to the assignment of the three largest hyperfine tensors to these three ring positions 2, 3, and 6 (methylene protons at position 5 can be excluded for reasons given below).

CH_3 tensors and the $^{\alpha}$H tensor can be distinguished by their ENDOR signal amplitudes and their anisotropies at low temperature: The $^{\alpha}$H tensor is known from high-field EPR to be strongly anisotropic with approximate axial symmetry. Its A_{XX} and A_{ZZ} components were determined by 95 GHz EPR between 8 and 10 MHz (*20*). Its A_{YY} component was observed to be less than 1 MHz. These properties can be clearly confirmed in general and accurately measured for the PQ-1$^{\cdot -}$ by high-field magnetoselective ENDOR: The two components A_{XX} and A_{ZZ} appear at the corresponding g_{XX} and g_{ZZ} positions as the largest couplings, but with low amplitude. The A_{YY} component must be searched for in the matrix region of the g_{YY} ENDOR spectrum, where it suffers from poor resolution due to overcrowding lines.

The methyl protons, which are still rotating freely when the temperature is lowered and therefore have relatively small hyperfine (HFS) anisotropy, show up with significantly larger ENDOR amplitudes than spatially fixed α-protons. Considering in addition the electron-donating inductive effect of the methylene group at position 5, the larger of the two CH_3 tensors is expected at position 2.

Unlike the methyl protons, the methylene protons at position β and the γ-proton on the isoprenoid chain are not expected to rotate freely in frozen solution. The chain will rather be locked in different conformations with strongly varying hyperfine tensors. This leads to a considerable broadening of corresponding ENDOR lines, so that the lines from the β and γ positions are too weak to be observed at this temperature (*25, 26*).

The remaining two HFS tensors must be assigned to the methyl protons in the two ϵ positions at the end of the isoprenoid chain. These groups again have small anisotropies on account of their rotational freedom and can therefore be observed at low temperatures.

All the above assignments are in agreement with RHF/INDO-SP spin-density calculations performed in our laboratory. These calculations predict the smaller $^{\epsilon}CH_3$ HFS tensor for the trans ϵ position.

The angles Φ_0 for the HFS tensors on the ring positions do not coincide with the angle of 30° between bond directions and the Y axis (see the structural formula) as one would expect for an isolated C–CH_3 or C–H fragment. This reflects the contribution of the large spin densities on the more remote O atoms to the dipolar HFS interaction.

CONCLUSION

The accuracy of the g-factor and hyperfine data obtained for the PQ-1$^{\cdot -}$ molecule demonstrate the feasibility of probing changes in structure and/or environment of quinone-like systems. Changes in hyperfine coupling constants and directions of tensor axes due to such perturbations are expected to be in the range between 0.1 and 1 MHz and between 1° and 10°, respectively (*20*). The required accuracy of the measurements can generally be expected for systems with g anisotropies above 1×10^{-3} and ENDOR linewidths below 0.2 MHz.

The results given in Table 1 show that W-band ENDOR allows one to determine hyperfine tensors (principal values and axis information) of quinone-type radicals in frozen solution with reasonable accuracy; i.e., it can be regarded as a promising tool for studies of solute–solvent interactions in biochemistry. On the other hand, elaborate computer simulation is required for analyzing the W-band ENDOR spectra, including a rigorous error analysis. Comparison with corresponding X-band ENDOR spectra is advisable for consistency tests because of the narrower linewidth in the X-band spectra.

Pulsed W-band EPR/ENDOR measurements (*9, 28*) are being performed on a whole series of semiquinone anion radicals with the aim to systematically determine relaxation tensors and hyperfine structures. In addition, W-band proton ENDOR studies on frozen solutions of perdeuterated quinone systems in protonated solvents are under way in order to determine the anisotropic hyperfine interactions of hydrogen bonds with the matrix.

ACKNOWLEDGMENTS

The excellent machine shop work of Mr. J. Claus and his support in the construction of the 3 mm ENDOR cavity are gratefully acknowledged. We thank J. T. Törring (Institute of Experimental Physics, FUB) for his expert programming and interfacing of the computer-controled high-field EPR/ENDOR experiments and C. Geßner (Max-Volmer-Institute, TUB) for helpful discussions. This work was supported by the Deutsche Forschungsgemeinschaft (SFB 337 and SFB 312).

REFERENCES

1. G. Rist and J. S. Hyde, *J. Chem Phys.* **49,** 2449 (1968); **50,** 4532 (1969); **52,** 4633 (1970).
2. J. Hüttermann, *Biol. Magn. Reson.* **13,** 219 (1993).
3. B. M. Hoffman, V. J. DeRose, P. E. Doan, R. J. Gurbiel, A. L. Houseman, and J. Telser, *Biol. Magn. Reson.* **13,** 151 (1993).
4. Ya. S. Lebedev, *in* "Modern Pulsed and Continuous-Wave Electron Spin Resonance" (L. Kevan and M. K. Bowman, Eds.), p. 365, Wiley, New York, 1990.
5. K. Möbius, *Biol. Magn. Reson.* **13,** 253 (1993).
6. O. Burghaus, M. Rohrer, T. Götzinger, M. Plato, and K. Möbius, *Meas. Sci. Technol.* **3,** 765 (1992).
7. O. Burghaus, E. Haindl, M. Plato, and K. Möbius, *J. Phys. E Sci. Instrum.* **18,** 294 (1985).

8. O. Burghaus, A. Toth-Kischkat, R. Klette, and K. Möbius, *J. Magn. Reson.* **80,** 383 (1988).
9. T. F. Prisner, M. Rohrer, and K. Möbius, *Appl. Magn. Reson.* **7,** 167 (1994).
10. V. V. Klimov, E. Dolan, E. R. Shaw, and B. Ke, *Proc. Natl. Acad. Sci. USA* **77,** 7227 (1980).
11. J. Forrer, A. Schweiger, and Hs. H. Günthard, *J. Phys. E Sci. Instrum.* **10,** 470 (1977).
12. K. Möbius and R. Biehl, *in* "Multiple Electron Resonance Spectroscopy" (M. M. Dorio and J. H. Freed, Eds.), p. 475, Plenum, New York, 1979.
13. S. Pfenninger, Ph.D. Thesis, ETH Zürich, 1991.
14. M. Peric and A. Dulcic, *J. Phys. E Sci. Instrum.* **14,** 700 (1980).
15. J.-P. Willems, A. A. Klaassen, E. J. Reijerse, G. E. Janssen, and E. deBoer, *Rev. Sci. Instrum.* **63,** 5362 (1992).
16. F. Bohlmann and K.-M. Kleine, *Chem. Ber.* **99,** 885 (1966).
17. C. P. Poole Jr. and H. A. Farach, "The Theory of Magnetic Resonance," p. 103, Wiley, New York, 1972.
18. C. G. Hurst, T. A. Henderson, and R. W. Kreilick, *J. Am. Chem. Soc.* **107,** 7294 (1985).
19. S. P. Greiner and R. W. Kreilick, *J. Magn. Reson.* **100,** 43 (1992).
20. O. Burghaus, M. Plato, M. Rohrer, K. Möbius, F. MacMillan, and W. Lubitz, *J. Phys. Chem.* **97,** 7639 (1993).
21. N. M. Atherton, "Electron Spin Resonance," p. 140, Wiley, New York, 1973.
22. H. J. Nussbaumer, "Fast Fourier Transform and Convolution Algorithms," Springer, New York, 1982.
23. R. Zurmühl, "Praktische Mathematik," p. 260, Springer, New York/Berlin, 1965.
24. K. Möbius, H. van Willigen, and A. H. Maki, *Mol. Phys.* **20,** 289 (1971).
25. F. MacMillan, Ph.D. Thesis, FU Berlin, 1993.
26. G. Feher, R. A. Isaacson, M. Y. Okamura, and W. Lubitz, *in* "Antennas and Reaction Centers of Photosynthetic Bacteria" (M. E. Michel-Beyerle, Ed.), p. 174, Springer, Berlin, 1985.
27. M. Rohrer, Diploma Thesis, Department of Physics, FU Berlin, 1991.
28. M. Rohrer, T. F. Prisner, P. Gast, and K. Möbius, *Chem. Phys. Lett.*, to appear (1995).